Two-dimensional band dispersion and momentum-resolved lifetime of the image-potential state on graphite studied by angle-resolved multiphoton photoemission spectroscopy

Kazutoshi Takahashi,* Junpei Azuma, and Masao Kamada
Synchrotron Light Application Center, Saga University, Saga 840-8502, Japan
(Received 15 December 2011; published 29 February 2012)

We studied the image-potential state (IPS) on a highly oriented pyrolitic graphite surface by means of angle-resolved multiphoton photoemission spectroscopy. The free-electron–like dispersion of IPSs with $n = 1$, 2, and 3 is observed for the first time with high energy and momentum resolution. From the dependence of the spectral intensity on the excitation density and comparisons with the energy diagram, it is suggested that IPSs are populated by the $k_{//}$-conserved transition from the σ-band and the indirect transition from the π-band. The linear dependence of the intrinsic line width on the energy suggests a contribution of intraband relaxation within the IPS band.

DOI: 10.1103/PhysRevB.85.075325 PACS number(s): 73.20.−r, 73.50.Gr, 78.47.−p, 81.05.uf

I. INTRODUCTION

Recently, extensive studies have been conducted on the electronic state of graphene due to its fascinating electronic structure or transport properties.[1] However, many concerns to date have been paid mainly to the occupied electronic state close to the Fermi level, which is located at the $\overline{\mathrm{K}}$ point of the surface Brillouin zone. In addition to knowledge about the occupied electronic state at thermal equilibrium, transient electron dynamics in unoccupied electronic states are also of great importance, since electrons excited to unoccupied states play important roles in electrical and optical properties. It is also very important to investigate the unoccupied electronic state of graphite, which is a relative material of graphene. One of the most interesting features in the unoccupied region is the interlayer state. It has been characterized by an interlayer dispersion and a maximum charge density between sp^2-hybridized carbon planes.[2] Experimental observations of the interlayer state have been reported by inverse photoemission spectroscopy,[3] near-edge x-ray absorption fine-structure spectroscopy,[4,5] and very-low-energy electron-diffraction measurements.[6] Recent theoretical work[7] has argued that the widely discussed interlayer band in graphite is a consequence of the intersheet hybridization of the first even image-potential state on each carbon sheet.

The image-potential state (IPS) is general concept and well known for the semi-infinite metal/vacuum interface, where an electron is trapped in front of the surface by an attracting force with its image charge.[8] Experimentally, the dynamics of IPS on many metal surfaces, including surfaces covered by adsorbates or metallic overlayers, have been studied with two-photon photoemission (2PPE) spectroscopy.[9] While the existence of IPS has been reported for highly oriented pyrolitic graphite (HOPG)[10] and Chemical-Vapor-Deposition-grown nanographene on Pt(111),[11] any experimental work with energy resolution sufficiently high enough to discuss the details of IPS, such as line shape, in-plane band dispersion, and other IPSs with larger quantum number (n), has not been reported. To develop further understanding of the electronic properties of graphene and related materials, it is important to obtain detailed knowledge of unoccupied electronic states and their dynamics, including the excitation and relaxation processes.

In this work, we studied in-plane band dispersion and the dynamics of IPS on HOPG by means of angle-resolved multiphoton photoemission (AR-MPPE) spectroscopy. IPSs with $n = 1$, 2, and 3 show parabolic band dispersions with an effective mass of unity. Possible multiphoton excitation processes for IPS are discussed from results of the dependence of the spectral intensity on the excitation density and the energy difference between the IPS band and occupied bulk bands. We also performed a detailed line-shape analysis of the IPS peak measured with sufficiently high energy resolution and found that the intrinsic line width of IPS with $n = 1$ depends linearly on the energy, suggesting a contribution from intraband relaxation within the parabolic IPS band.

II. EXPERIMENT

Experiments were performed on a beamline BL13 at the Saga Light Source. Details of the beamline have been published elsewhere.[12,13] The HOPG sample was cleaved in air before quick loading into a load-lock chamber, and the surface was cleaned by *in-situ* heating at 670 K for 14 h in the preparation chamber at about 2×10^{-8} Pa. The surface cleanliness was checked by core-level and valence band photoemission measurements with synchrotron radiation. We used photon energies of 670 and 130 eV for core-level and valence band photoemission measurements, respectively. No contamination-related feature, such as an O 1s peak, was found in the core-level photoemission spectra. Angle-resolved valence photoemission spectra showed clear dispersions, which were superimposed spectral features originating from $\Gamma K(AH)$ and $\Gamma M(AL)$ high-symmetry directions. The work function was determined by the low-energy cutoff of the photoemission spectra. The obtained work function of 4.49 eV fits well with the literature value of 4.5 ± 0.1 eV,[10] while it is slightly smaller than the value of 4.7 eV for a single crystal surface.[14]

The laser system used in the present experiment was a Ti:sapphire regenerative amplifier, which can generate ultrashort pulses less than 200 fs in duration. The wavelength, repetition rate, and pulse energy of the fundamental were 810 nm, 300 kHz, and 2 μJ, respectively. The excitation densities of frequency-doubled ($2h\nu$) and frequency-

tripled ($3h\nu$) light were varied in the range of 2.6–14 and 0.8–4.8 nJ/mm^2, respectively. The Fermi energy and the energy resolution were estimated by measurement for the Fermi edge of the Pt reference. The overall instrumental energy resolution was estimated as 79 ± 3 meV. The acceptance angle of the photoelectron spectrometer was set to ±0.5°.

III. RESULTS AND DISCUSSION

Figure 1 shows MPPE spectra at normal emission geometry, which are excited with $2h\nu$ (b) and $3h\nu$ (c) pulses, and the energy diagram of the photoemission from IPSs (a). The horizontal axis is shown by electron kinetic energy with respect to the vacuum level of the sample. Characteristic peaks are observed at 2.11, 2.82, and 2.94 eV in the MPPE spectrum with $2h\nu$ excitation. The MPPE spectrum with $3h\nu$ pulse shows a sharp peak at 3.65 eV in addition to a broad peak around 1.7 eV as shown in Fig. 1(c). These peaks have been found to suppress their intensities with excitation of s-polarized geometry (spectra are not shown here), according to the electric dipole selection rules for excitation from IPS and bulk π^*-band, which are excited by a component of the electric field perpendicular to the surface. The binding energies of the IPSs relative to the vacuum level are described by $E_b(n) = 0.85/(n + a)^2$, with units of eV, where n is the quantum number, and a is the quantum defect.[8] The measured binding energies of the IPSs lead a quantum defect of $a = -0.07 \pm 0.02$. This value is not too far off from the vanishing quantum defect reported by Lehmann *et al.*,[10] suggesting that the lowest unoccupied σ-band is located at close to the IPS and

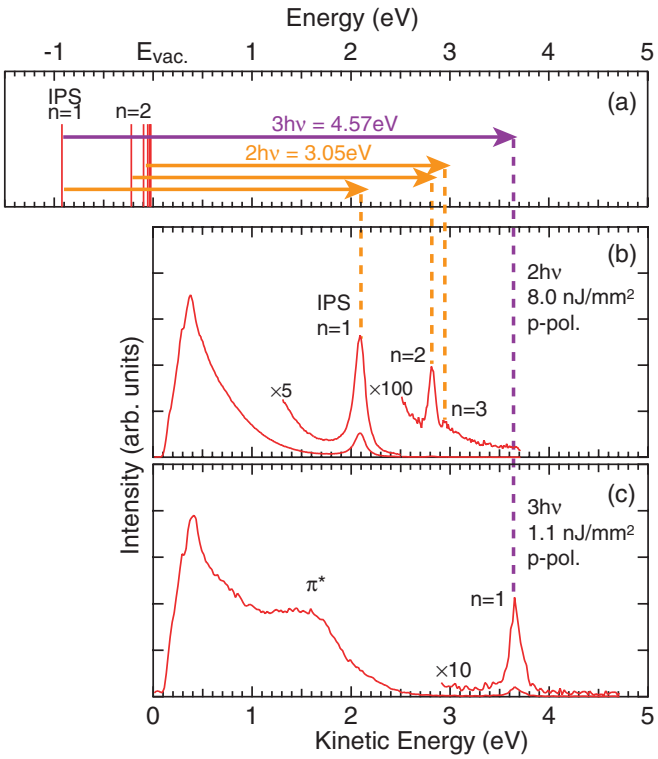

FIG. 1. (Color online) (a) Energy diagram of the electron excitation from the IPS by $2h\nu$ and $3h\nu$ pulses. (b) Normal emission spectrum excited with a $2h\nu$ pulse as well as (c) that with a $3h\nu$ pulse.

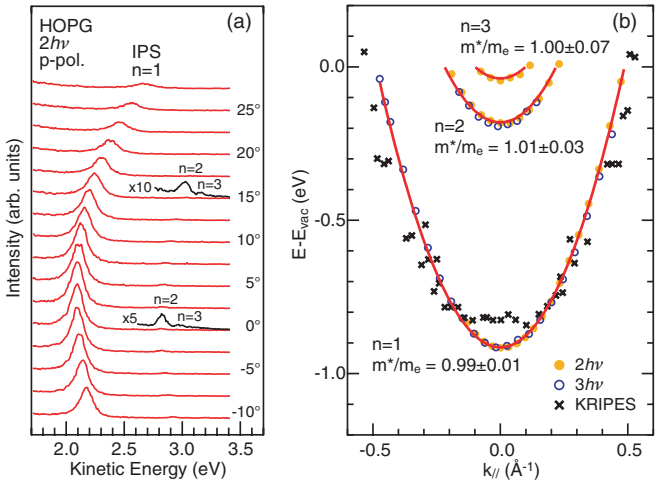

FIG. 2. (Color online) (a) Angle-resolved spectra with $2h\nu$ excitation at polar emission angles from −10° to 27.5°. Five- and ten-times magnified spectra are also shown for emission angles of 0° and 15°, respectively. (b) Two-dimensional band dispersion of IPS with $n = 1$, 2, and 3 determined from the AR-MPPE spectra.

is of particular relevance for the decay channel of the IPS. This assignment is also consistent with the recent theoretical study describing that interlayer band in graphite is evolved by the intersheet hybridization of the first even IPS on each graphene sheet.[7]

Figure 2(a) shows the AR-MPPE spectra with $2h\nu$ excitation at polar emission angles from −10° to 27.5°. The peak from $n = 1$ IPS shows the clear dispersion to the higher kinetic energy side with increasing emission angle. Precise determination of the peak positions and direct observation of the dispersions of IPSs with $n = 2$ and 3 are some of the benefits of the recent technological progress in photoelectron spectrometry with high efficiency and high energy resolution. To our knowledge, this is the first report on experimental band dispersions of the IPSs with $n = 2$ and 3 on graphite. The spectra for the kinetic energy region corresponding to the $n = 2$ and 3 IPSs are shown as five and ten times magnified spectra at 0° and 15°. Two-dimensional band dispersions of the IPSs with $n = 1$, 2, and 3, which are determined from the AR-MPPE spectra, are shown in Fig. 2(b). AR-MPPE measurement was also performed with $3h\nu$ excitation (spectra are not shown here). Solid and open circles show the results with the $2h\nu$ and $3h\nu$ excitation, respectively. While it was difficult to distinguish the IPS of $n = 3$ in the spectra with $3h\nu$ excitation, both results fit well with each other. Solid lines in Fig. 2(b) show the results of least-square fittings to the experimental band dispersions assuming parabolic dispersion, which reproduce the observed dispersion and give effective mass m^*/m_e of 0.99 ± 0.01, 1.01 ± 0.03, and 1.00 ± 0.07 for IPSs with $n = 1$, 2, and 3, respectively. These values indicate that the effective mass of the IPSs with $n = 1$, 2, and 3 is equal to the value of the free electrons within the errors from least-square fittings. Figure 2(b) also indicates that the bottom of the $k_{//}$ dispersion curves for IPSs is located at the $\Gamma(A)$ point. An unoccupied electronic state that shows the $k_{//}$ dispersion and is located just below the vacuum level has been reported as IPS with $n = 1$ from a momentum-resolved

inverse photoemission (KR-IPES) study.[15] Its experimental data points are also shown in Fig. 2(b) as crossed markers (×). IPSs with the quantum number larger than 2 were not resolved in the KR-IPES study. The effective mass derived from the KR-IPES has been reported as 1.3, which is slightly larger than that in the present study. The different bottom position and the effective mass of the IPS band by KR-IPES apparently originate from insufficient energy resolution and/or the larger acceptance angle than those in our equipment.

It should be noted that the values of m^* for the IPSs with $n = 1$, 2, and 3 are equal to that for the free electrons. Recent 2PPE studies for IPS on noble metal surface have reported that the modification of the effective mass of the IPS occurs via coupling to the bulk electronic state[16] or scattering with the hot-electron gas.[17,18] On the other hand, the observed m^* values of IPS on HOPG suggest negligible coupling of the IPSs to bulk electronic states or hot-electron gas. This is consistent with a large separation between the projected bulk band and the parabolic IPS bands in energy and momentum space.

In order to elucidate the excitation process to the IPS, the dependence of the spectral intensity on excitation density was examined in detail. The intensity of the $n = 1$ IPS was evaluated by the area of the peak. Figure 3(a) shows the plots of the IPS intensity against the excitation density at normal emission geometry with $3h\nu$ and $2h\nu$, and at the emission angle of 25° with a $2h\nu$ pulse. Solid lines in Fig. 3(a) show the results of least-square fittings with a power law against the excitation density considering an exponent as a fitting parameter. The result for $3h\nu$ excitation at normal emission geometry is shown by a line with a slope of 2.5 in a single logarithmic plot in Fig. 3(a). On the other hand, the results for $2h\nu$ excitation are shown by a line with a slope of 3.9. There are no noticeable differences between emission angles of 0° and 25° at $2h\nu$ excitation. These exponent values give insights for the excitation processes and are discussed later.

Figure 3(b) shows the energy diagram of the expected multiphoton photoemission process via IPS. Observed band dispersions of IPS are shown by solid lines. The projected bulk bands from the theoretical calculation,[19] which are consistent with the observed bulk band-dispersion, are also shown by filled area. No occupied surface state such as the Shockley-type surface state on a noble metal (111) surface, which causes the resonant excitation between the surface state and IPS, is reported on the graphite surface. The excitation from IPS, which corresponds to the intermediate state to the final state above the vacuum level, can be explained by a one-photon transition, as shown in the energy diagram of Fig. 1(a). As shown in Fig. 2(b), the bottom of the $n = 1$ IPS is located at 3.57 eV above the Fermi level at $k_{//} = 0$. Thus, the $k_{//}$-conserved one-photon direct transition from the occupied bulk band around the K or M point is not adequate to explain the excitation process to IPS. Phonon-assisted indirect excitation from the bulk π-band around the $K(H)$ point ranging between the Fermi level and a binding energy of about 1.0 eV is one of the presumable candidates for the excitation process to IPS. This process should contribute as the quadratic dependence of IPS peak intensity on the excitation density. However, the observed exponent value of 2.5 indicates the existence of cubic dependence due to a three-photon transition process in addition to the quadratic dependence due to the above indirect excitation. So, other excitation processes involving the two-photon absorption must be considered as the excitation process from the occupied bulk state to IPS. While the $k_{//}$-conserved one-photon transition from the π-band around the Γ point is impossible due to the energy difference between the π-band and the IPS, the two-photon transition from the σ-band to the IPS can be allowed by $3h\nu$ pulses. The observed exponent value of 2.5 may be explained by the coexistence of the one-photon indirect transition to the IPS from the π-band and the $k_{//}$-conserved direct two-photon transition from the σ-band, and the subsequent excitation to the final state above the vacuum level from the IPS by a one-photon transition.

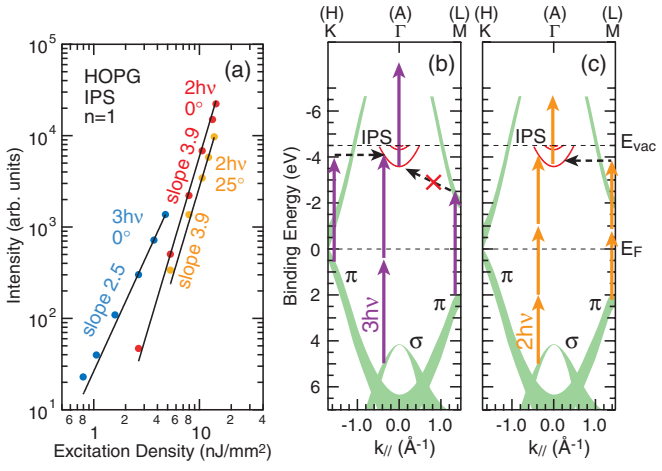

FIG. 3. (Color online) (a) Plots of the IPS intensity against the excitation density at normal emission geometry with $3h\nu$ and $2h\nu$ pulses, and at an emission angle of 25° with a $2h\nu$ pulse. Solid lines show the results of a least-square fitting with a power law. (b) The energy diagram of the expected multiphoton photoemission process via IPS with $2h\nu$ excitation. (c) Same as (b) with $3h\nu$ excitation.

Similar discussion gives insights for the multiphoton photoemission process via IPS under the $2h\nu$ excitation. The expected energy diagram is shown in Fig. 3(c). The $k_{//}$-conserved transition from the σ-band to the IPS is the most presumable excitation process to populate IPS, which corresponds to an exponent value of 4. From consideration of the energy difference between the IPS and projected bulk band originating from the bulk π-band near the K and M points, an indirect transition from the π-band to the IPS with two-photon absorption cannot be excluded as the excitation process to IPS, because the obtained exponent value is slightly smaller than 4. A smaller exponent value of about 2.5 has been reported before for the $n = 1$ IPS, which was interpreted to indicate the onset of the indirect transition from the π-band to the IPS with two-photon absorption.[10] In addition to the previously reported indirect transition from the π-band, present dependence on the excitation density strongly suggests the onset of a $k_{//}$-conserved transition from the σ-band to the IPS. More detailed measurements, such as the dependence on the excitation photon energy, will confirm these assignments about the excitation process.

In order to elucidate the dynamics of electrons transiently populated to IPS, we discuss the lifetime of the electron in IPS, which can be obtained from intrinsic line-width analysis. The 2PPE line width is given by $\Gamma = \hbar(1/T_1 + 2/T_2^*)$, where T_1 is

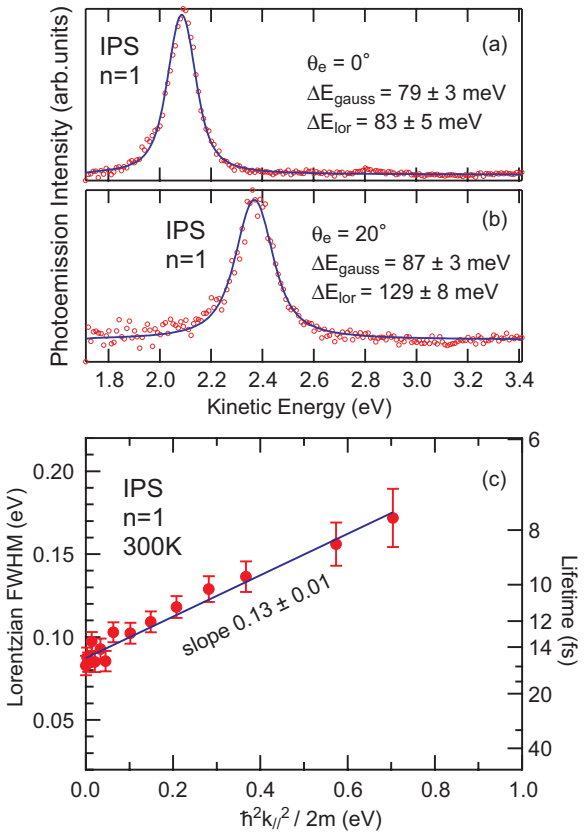

FIG. 4. (Color online) (a) The line-shape analysis of the $n = 1$ IPS measured at 0° as well as (b) 20°. (c) Experimental intrinsic line width and associated transversal relaxation time of $n = 1$ IPS. Horizontal axis is the kinetic energy of parallel motion.

the energy relaxation time, and $T_2{}^*$ accounts for pure dephasing such as quasi-elastic scattering by defects.[20] The transversal relaxation-time T_2 is also related to the intrinsic line width by $\Gamma = 2\hbar/T_2$. The line-shape analyses of the $n = 1$ IPS measured at 0° and 20° are shown in Figs. 4(a) and 4(b), respectively. The IPS peak has been fitted by a single Lorentzian peak that is convoluted by a Gaussian representing the instrumental broadening. In addition to the total energy resolution ΔE of the measurement, the finite angular resolution $\Delta\theta$ also contributes to the broadening of the measured line width, because the finite angular resolution results in a finite momentum resolution $\Delta k_{//}$, and IPS shows a parabolic dispersion with an effective mass that is the same as a free electron. A vector sum of the extrinsic line width due to the energy resolution and momentum resolution has been used as the FWHM of the Gaussian in the line-shape analysis of the spectrum at each emission angle. From least-mean-square-fitting procedures, intrinsic line widths of 83 ± 5 and 129 ± 8 meV have been obtained for the spectra at 0° and 20°, respectively. In Fig. 4(c), the obtained Lorentzian line width and associated transversal relaxation time are plotted as a function of the kinetic energy of parallel motion $\hbar^2 k_{//}{}^2/2m$. The error bars in Fig. 4(c) refer to the uncertainty arising in the determination of the line width from the fitting procedure. As shown in Fig. 4(c), IPS shows a shorter lifetime at larger $k_{//}$. The evaluated transversal relaxation time at the bottom of the IPS band is about 16 fs, which is larger than T_2 value of 8 ± 2 fs in the literature.[10] It has been also reported that the energy relaxation time is 40 fs from the transient population measurement for $n = 1$ IPS, which implies an elastic-scattering contribution to the intrinsic line width of about 154 meV. The difference between the intrinsic line width in our results and previous studies might stem from the different sample quality, such as surface defect density. The larger amount of surface defects in the microcrystalline distribution of HOPG will cause the higher rate of defect-induced quasi-elastic scattering and a shorter dephasing lifetime $T_2{}^*$. The defect-induced scattering of IPS electrons has been reported as the 2PPE line width of IPS on Cu(111) at very low Na dosage.[21] In conjunction with the quantitative analysis in the previous report,[21] a surface defect density of about 0.005 ML will cause broadening of about 70 meV. Another candidate that might cause different intrinsic line widths is the difference in the excitation process. From the exponent value of 4, the $k_{//}$-conserved transition from the σ-band to the IPS is suggested as a presumable excitation process to populate the IPS in the present work, while indirect transitions from the π-band to the IPS have been suggested from the exponent value smaller than 3 by Lehmann *et al.*[10] Rapid dephasing will be expected for the excitation process involving indirect transitions because momentum conservation implies that the indirect transition from the π-band to the IPS destroys the coherence of the excitation. The solid line in Fig. 4(c) is a linear fit to the Lorentzian line width versus the kinetic energy of parallel motion, which gives a slope of 0.13. Similar shortening of the lifetime versus increasing $k_{//}$ has been reported for the IPS on Cu(100)[22] and Ag(100)[23] surfaces. It has been suggested that the intraband scattering within the parabolic band can explain the pronounced decrease of the lifetime at finite parallel momentum.[22] Similarly, the present linear dependence of the intrinsic line width on the energy could be accounted for by intraband relaxation within the image-state band on HOPG.

The present results show that the AR-MPPE technique with high energy and momentum resolution can clarify band dispersions of IPSs with higher quantum numbers and the momentum-resolved information about their dynamics. This technique will be able to provide detailed understanding concerning the two-dimensional dispersion and the dynamics of IPSs on graphene and related materials. The electron dynamic of IPS on graphite obtained here should also be compared with that on graphene, where clear dependencies on the layer thickness or the coupling to the substrate are expected because the establishment of an interlayer state will modify the decay channel from IPSs. The dependence on the doping characteristic is also of interest. These comprehensive experiments will provide improved understandings about the excited electronic states that play important roles in electrical and optical properties of graphene and related materials.

IV. CONCLUSION

We have reported the direct measurement of the free-electron–like parabolic dispersion of IPSs with $n = 1$, 2, and 3 using AR-MPPE spectroscopy with sufficiently high energy resolution. From the dependence on the excitation density, it is

suggested that IPSs are populated by the $k_{//}$-conserved direct transition from the σ-band and the indirect transition from the π-band near the boundary of the surface Brillouin zone. The dependence of IPS line width on the momentum parallel to surface has been determined from a detailed line-shape analysis of the IPS peak. The linear dependence of intrinsic line width on the energy suggests that intraband relaxation within the IPS band contributes to the inelastic scattering process. This AR-MPPE technique with high energy and momentum resolution can be widely applicable to the study of the momentum-resolved electron dynamics on graphene and related materials.

ACKNOWLEDGMENTS

This work was supported by Grants-in-Aid for Scientific Research, and the MEXT Joint Project of Research and Development of Innovative Bio-, Nano- and Environmental Technologies Using Synchrotron Light through Wide-Range Cooperation and Integration.

*Corresponding author: ktaka@cc.saga-u.ac.jp

[1] K. S. Novoselov, A. K. Geim, S. V. Morozov, D. Jiang, Y. Zhang, S. V. Dubonos, I. V. Grigorieva, and A. A. Firsov, Science **306**, 666 (2006).

[2] M. Posternak, A. Baldereschi, A. J. Freeman, and E. Wimmer, Phys. Rev. Lett. **52**, 863 (1984).

[3] Th. Fauster, F. J. Himpsel, J. E. Fischer, and E. W. Plummer, Phys. Rev. Lett. **51**, 430 (1983).

[4] D. A. Fischer, R. M. Wentzcovitch, R. G. Carr, A. Continenza, and A. J. Freeman, Phys. Rev. B **44**, 1427 (1991).

[5] D. Pacilé, M. Papagno, A. Fraile Rodríguez, M. Grioni, L. Papagno, Ç. Ö. Girit, J. C. Meyer, G. E. Begtrup, and A. Zettl, Phys. Rev. Lett. **101**, 066806 (2008).

[6] V. N. Strocov, P. Blaha, H. I. Starnberg, M. Rohlfing, R. Claessen, J.-M. Debever, and J.-M. Themlin, Phys. Rev. B **61**, 4994 (2000).

[7] V. M. Silkin, J. Zhao, F. Guinea, E. V. Chulkov, P. M. Echenique, and H. Petek, Phys. Rev. B **80**, 121408 (2009).

[8] P. M. Echenique and J. B. Pendry, J. Phys. C **11**, 2065 (1978).

[9] P. M. Echenique, R. Berndt, E. V. Chulkov, Th. Fauster, A. Goldmann, and U. Höfer, Surf. Sci. Rep. **52**, 219 (2004).

[10] J. Lehmann, M. Merschdorf, A. Thon, S. Voll, and W. Pfeiffer, Phys. Rev. B **60**, 17037 (1999).

[11] I. Kinoshita, D. Ino, K. Nagata, K. Watanabe, N. Takagi, and Y. Matsumoto, Phys. Rev. B **65**, 241402 (2002).

[12] K. Takahashi, Y. Kondo, J. Azuma, and M. Kamada, J. Electron Spectrosc. Relat. Phenom. **144-147**, 1093 (2005).

[13] K. Takahashi, J. Azuma, S. Tokudomi, and M. Kamada, AIP Conference Proceedings **879**, 1218 (2007).

[14] R. Claessen, H. Carstensen, and M. Skibowski, Phys. Rev. B **38**, 12582 (1988).

[15] I. Schäfer, M. Schlüter, and M. Skibowski, Phys. Rev. B **35**, 7663 (1987).

[16] D. F. Padowitz, W. R. Merry, R. E. Jordan, and C. B. Harris, Phys. Rev. Lett. **69**, 3583 (1992).

[17] G. Ferrini, C. Giannetti, G. Galimberti, S. Pagliara, D. Fausti, F. Banfi, and F. Parmigiani, Phys. Rev. Lett. **92**, 256802 (2004).

[18] S. Pagliara, G. Ferrini, G. Galimberti, E. Pedersoli, C. Giannetti, C. Rozzi, and F. Parmigiani, Surf. Sci. **602**, 2983 (2008).

[19] R. C. Tatar and S. Rabii, Phys. Rev. B **25**, 4126 (1982).

[20] T. Hertel, E. Knoesel, M. Wolf, and G. Ertl, Phys. Rev. Lett. **76**, 535 (1996).

[21] X. Y. Wang, R. Paiella, and R. M. Osgood Jr., Phys. Rev. B **51**, 17035 (1995).

[22] W. Berthold, U. Höfer, P. Feulner, E. V. Chulkov, V. M. Silkin, and P. M. Echenique, Phys. Rev. Lett. **88**, 056805 (2002).

[23] G. Ferrini, C. Giannetti, D. Fausti, G. Galimberti, M. Peloi, G. P. Banfi, and F. Parmigiani, Phys. Rev. B **67**, 235407 (2003).